J|A|C|S

A R T I C L E S

Enzyme-Catalyzed Bio-Pumping of Electrons into Au-Nanoparticles: A Surface Plasmon Resonance and Electrochemical Study

Oleg Lioubashevski,[†] Vladimir I. Chegel,[‡] Fernando Patolsky,[†] Eugenii Katz,[†] and Itamar Willner*,[†]

Contribution from the Institute of Chemistry, The Farkas Center for Light-induced Processes, The Hebrew University of Jerusalem, Jerusalem 91904, Israel, and Institute of Physics of Semiconductors, National Academy of Science of Ukraine, Prospect Nauki, 45, Kiev, Ukraine

Received February 10, 2004; E-mail: willnea@vms.huji.ac.il

Abstract: The enzyme glucose oxidase (GOx) is reconstituted on a flavin adenin dinucleotide (FAD, **1**) cofactor-functionalized Au-nanoparticle (Au-NP), 1.4 nm, and the GOx/Au-NP hybrid is linked to a bulk Au-electrode by a short dithiol, 1,4-benzenedithiol (**2**), or a long dithiol, 1,9-nonanedithiol (**3**), monolayer. The reconstituted GOx/Au-NP hybrid system exhibits electrical communication between the enzyme redox cofactor and the Au-NP core. Because the thiol monolayers provide a barrier for electron tunneling, the electron transfer occurring upon the biocatalytic oxidation of glucose results in the Au-NPs charging. The charging of the Au-NPs alters the plasma frequency and the dielectric constant of the Au-NPs, thus leading to the changes of the dielectric constant of the interface. These are reflected in pronounced shifts of the plasmon angle, θ_P, in the surface plasmon resonance (SPR) spectra. As the biocatalytic charging phenomenon is controlled by the concentration of glucose, the changes in the θ_P values correlate with the concentration of glucose. The biocatalytic charging process is characterized by following the differential capacitance of the GOx/Au-NP interface and by monitoring the potential generated on the bulk Au-electrode. The charging of the GOx/Au-NPs is also accomplished in the absence of glucose by the application of an external potential on the electrode, that resulted in similar plasmon angle shifts. The results allowed us to estimate the number of electrons stored per Au-NP at variable concentrations of glucose in the presence of the two different thiol linkers.

Introduction

The organization of molecular components in nanoscale structures on surfaces is a challenging topic in modern science. Various possible applications of such systems in the development of information storage and processing, photovoltaics, and sensor devices have been suggested.[1] Biomaterials, such as proteins/enzymes, antigens/antibodies, receptors, and DNA, which demonstrate unique catalytic or recognition properties, could be important components of such nanoscale systems.[2]

The electrochemical activation of enzymes[3,4] is a common practice in bioelectrochemistry and in the development of biosensor devices[5] and biofuel cells.[6] Most of the electrically

activated enzyme-electrodes, however, lead to an amperometric response as a result of the biocatalyzed oxidation or reduction of the respective substrates. The potentiometric analysis of substrates at enzyme-electrodes is usually accomplished by controlling the electrode potential by one of the reacting substrates,[7] for example, the depletion of oxygen,[8] or by chemical changes induced by the reaction products, for example, altering the pH of the system[9] as a result of the biocatalytic process.

The electrical contacting of redox enzymes and electrode supports was achieved by the surface reconstitution of apo-

† The Hebrew University of Jerusalem.
‡ National Academy of Science of Ukraine.

(1) (a) Wei, Y. *Supramol. Sci.* **1998**, *5*, 723−731. (b) Nitzan, A. *Annu. Rev. Phys. Chem.* **2001**, *52*, 681−750. (c) Stan, M. R.; Franzon, P. D.; Goldstein, S. C.; Lach, J. C.; Ziegler, M. M. *Proc. IEEE* **2003**, *91*, 1940−1957. (d) Service, R. F. *Science* **2003**, *302*, 556−558. (e) Park, J. W.; Pasupathy, A. N.; Goldsmith, J. I.; Soldatov, A. V.; Chang, C.; Yaish, Y.; Sethna, J. P.; Abruna, H. D.; Ralph, D. C.; McEuen, P. L. *Thin Solid Films* **2003**, *438*, 457−461.
(2) (a) Davis, J. J. *Philos. Trans. R. Soc. London, Ser. A* **2003**, *361*, 2807−2825. (b) Willner, I. *Nat. Biotechnol.* **2001**, *19*, 1023−1024. (c) Willner, I.; Willner, B. *Trends Biotechnol.* **2001**, *19*, 222−230. (d) Willner, I. *Science* **2002**, *298*, 2407−2408.
(3) (a) Armstrong, F. A.; Wilson, G. S. *Electrochim. Acta* **2000**, *45*, 2623−2645. (b) Heller, A. *Acc. Chem. Res.* **1990**, *23*, 128−134. (c) Heller, A. *J. Phys. Chem.* **1992**, *96*, 3579−3587.

(4) (a) Willner, I.; Katz, E. *Angew. Chem., Int. Ed.* **2000**, *39*, 1180−1218. (b) Katz, E.; Shipway, A. N.; Willner, I. In *Encyclopedia of Electrochemistry*; Wilson, G. S., Ed.; Wiley-VCH: GmbH, Weinheim, Germany, 2002; Vol. 9, Chapter 17, pp 559−626.
(5) (a) Wang, J. *J. Pharm. Biomed. Anal.* **1999**, *19*, 47−53. (b) Schmidt, H.-L.; Schuhmann, W. *Biosens. Bioelectron.* **1996**, *11*, 127−135. (c) Willner, I.; Katz, E.; Willner, B. *Electroanalysis* **1997**, *13*, 965−977.
(6) (a) Katz, E.; Willner, I.; Kotlyar, A. B. *J. Electroanal. Chem.* **1999**, *479*, 64−68. (b) Barton, S. C.; Kim, H.-H.; Binyamin, G.; Zhang, Y.; Heller, A. *J. Am. Chem. Soc.* **2001**, *123*, 5802−5803. (c) Chen, T.; Barton, S. C.; Binyamin, G.; Gao, Z.; Zhang, Y.; Kim, H.-H.; Heller, A. *J. Am. Chem. Soc.* **2001**, *123*, 8630−8631. (d) Katz, E.; Shipway, A. N.; Willner, I. In *Handbook of Fuel Cells − Fundamentals, Technology, Applications*; Vielstich, W., Gasteiger, H., Lamm, A., Eds.; Wiley: New York, 2003; Vol. 1, Part 4, Chapter 21, pp 355−381. (e) Katz, E.; Willner, I. *J. Am. Chem. Soc.* **2003**, *125*, 6803−6813.
(7) (a) Kharitonov, A. B.; Zayats, M.; Alfonta, L.; Katz, E.; Willner, I. *Sens. Actuators, B* **2001**, *76*, 203−210. (b) Zayats, M.; Kharitonov, A. B.; Katz, E.; Willner, I. *Analyst* **2001**, *126*, 652−657.
(8) Rotariu, L.; Bala, C.; Magearu, V. *Anal. Chim. Acta* **2002**, *458*, 215−222.

enzymes on relay-cofactor units associated with electrodes.[10,11] For example, apo-glucose oxidase (apo-GOx) was reconstituted on a pyrroloquinoline quinone (PQQ)-flavin adenine dinucleotide (FAD) unit associated with a Au-electrode.[10] In this system, the PQQ molecule operated as an electron relay providing efficient vectorial electron transfer from the FAD cofactor reconstituted into the GOx enzyme to the electrode support. Recently, the electrical contacting of glucose oxidase (GOx) was accomplished by the reconstitution of the apo-GOx on a FAD-functionalized Au-nanoparticle (1.4 nm) that was linked to the Au-electrode surface by a dithiol monolayer.[12] This study indicated that the electron transfer from the FAD cofactor to the electrode support occurred through the Au-NP.

The quantum charging of Au-NP by electrochemical means is a subject of extensive research.[13] The optical spectra of Au-NPs show a localized surface plasmon (LSP) band in the region of 520−550 nm. The interactions of LSP of Au-NP and, specifically, of charged Au-NP with the surface plasmon (SP) excited on the surface of the bulk gold are of special interest and could be studied by the surface plasmon resonance (SPR) technique.

Surface plasmon resonance (SPR) spectroscopy is a versatile method to probe and characterize physicochemical changes on thin films such as Au-surfaces.[14] The ability to probe chemical modifiers on surfaces by means of SPR turned the method into a useful analytical tool, and different biorecognition processes, such as protein binding or DNA hybridization, were followed by SPR measurements.[15,16] In most of these studies, the chemical modification alters the refractive index and film thickness, and these changes affect the resulting SPR spectra. The surface plasmons (SP) are resonantly excited surface electromagnetic waves, that propagate along planar metal/dielectric interfaces and are strongly localized in the vicinity of the interface. In the presence of a metal-NP layer, part of the SP energy is transferred outside through scattering within the NP layer. The interaction between the LSP associated with the noble metal NP and the SP on the metal−dielectric interface leads to a deformation of the dispersion curve of the SP and to a shift in the plasmon

resonance angle.[17] Indeed, Au-nanoparticles have been extensively used for the detection of bioaffinity binding processes by virtue of the nanoparticle-enhanced SPR changes.[18] A significant enhancement of the SPR signal was achieved for immunosensing[19] and DNA sensing[20] when Au-nanoparticles were used as labels. Also, the enhanced SPR read-out of redox reactions and bioelectrocatalytic processes was observed when the redox components that associated and dissociated to and from the electrode surface, respectively, were coupled with Au-nanoparticles.[21]

It is well established that charging the Au-NP core with electrons, or the removal of electrons from the Au-NP, results in significant shifts in the LSP band.[22] These spectral shifts of LSP band position were attributed to changes in the plasma frequency caused by the charge density increase resulting from the electrolytical charging of the metal NP.[22b,c] For example, turning a Au-NP to an electron-deficient state by altering the potential from −0.16 to 0.82 V (vs a Ag quasi-reference electrode) causes the LSP band to shift to lower energies.[22c] The charging of the Au-NP is anticipated to affect the coupling between the LSP and the SP of the bulk metal film, and thus changes in the SPR spectrum are expected upon the charging of the Au−NP. Indeed, in a recent study,[23] we were able to demonstrate the photoelectrochemical charging of Au-NPs (mean diameter 2.3 nm) linked to a Au-surface through a supporting cystamine monolayer by means of the photonic excitation of CdS-NPs linked to the Au-NPs. The charging of the Au-NPs in the Au-NP/CdS-NP array was followed by SPR spectroscopy and electrochemical measurements. The supporting organic layer provided a dielectric medium between the Au-NPs and the Au-electrode, and this allowed the electron tunneling from the Au-NPs to the bulk electrode, thus limiting the extent of the Au-NPs charging and the resulting changes of the SPR spectra. The electron tunneling efficiency decreases exponentially with the thickness of the dielectric layer, and the electron tunneling constant $\beta \approx 0.5-1.4$ Å^{-1} was reported.[24] Thus, for longer alkane chains as bridging units between the Au-NPs and the Au-surface, higher tunneling barriers for electron leakage to the surface should be expected, resulting in the enhanced accumulation of charges on the Au-NPs. The increased charging of the Au-NP will then yield a pronounced shift in the SPR spectra as a result of the coupling between the LSP and the charged Au-NP and the SP.

It is known that gold nanoparticles of size larger than 2 nm possess the plasmon band,[25] and the shift of the plasmon peak position as a result of nanoparticles charging on an electrode surface or in solution was demonstrated in numerous studies.[22]

(9) (a) Wang, J. Q.; Chou, J. C.; Sun, T. P.; Hsiung, S. K.; Hsiung, G. B. *Sens. Actuators, B* **2003**, *91*, 5−10. (b) Situmorang, M.; Gooding, J. J.; Hibbert, D. B.; Barnett, D. *Electroanalysis* **2001**, *13*, 1469−1474.

(10) (a) Willner, I.; Heleg-Shabtai, V.; Blonder, R.; Katz, E.; Tao, G.; Bückmann, A. F.; Heller, A. *J. Am. Chem. Soc.* **1996**, *118*, 10321−10322. (b) Katz, E.; Riklin, A.; Heleg-Shabtai, V.; Willner, I.; Bückmann, A. F. *Anal. Chim. Acta* **1999**, *385*, 45−58.

(11) (a) Raitman, O. A.; Katz, E.; Bückmann, A. F.; Willner, I. *J. Am. Chem. Soc.* **2002**, *124*, 6487−6496. (b) Raitman, O. A.; Patolsky, F.; Katz, E.; Willner, I. *Chem. Commun.* **2002**, 1936−1937. (c) Guo, L.-H.; McLendon, G.; Razafitrimo, H.; Gao, Y. *J. Mater. Chem.* **1996**, *6*, 369−374. (d) Zimmermann, H.; Lindgren, A.; Schuhmann, W.; Gorton, L. *Chem.-Eur. J.* **2000**, *6*, 592−599.

(12) Xiao, Y.; Patolsky, F.; Katz, E.; Hainfeld, J. F.; Willner, I. *Science* **2003**, *299*, 1877−1881.

(13) (a) Hicks, J. F.; Miles, D. T.; Murray, R. W. *J. Am. Chem. Soc.* **2002**, *124*, 13322−13328. (b) Hicks, J. F.; Zamborini, F. P.; Osisek, A. J.; Murray, R. W. *J. Am. Chem. Soc.* **2001**, *123*, 7048−7053. (c) Chen, S.; Murray, R. W. *J. Phys. Chem. B* **1999**, *103*, 9996−10000. (d) Hicks, J. F.; Zamborini, F. P.; Murray, R. W. *J. Phys. Chem. B* **2002**, *106*, 7751−7757.

(14) (a) Knoll, W. *Annu. Rev. Phys. Chem.* **1998**, *49*, 569−638. (b) Badia, A.; Arnold, S.; Scheumann, V.; Zizlsperger, M.; Mack, J.; Jung, G.; Knoll, W. *Sens. Actuators, B* **1999**, *54*, 145−165. (c) Homola, J.; Yee, S. S.; Gauglitz, G. *Sens. Actuators, B* **1999**, *54*, 3−15.

(15) (a) Rao, J.; Yan, L.; Xu, B.; Whitesides, G. M. *J. Am. Chem. Soc.* **1999**, *121*, 2629−2630. (b) Sasaki, S.; Nagata, R.; Hock, B.; Karube, I. *Anal. Chim. Acta* **199**8, *368*, 71−76. (c) Berger, C. E. H.; Greve, J. *Sens. Actuators, B* **2000**, *63*, 103−108.

(16) (a) Mullett, W. M.; Lai, E. P. C.; Yeung, J. M. *Methods* **2000**, *22*, 77−91. (b) Disley, D. M.; Cullen, D. C.; You, H. X.; Lowe, C. R. *Biosens. Bioelectron.* **1998**, *13*, 1213−1225. (c) Kruchinin, A. A.; Vlasov, Y. G. *Sens. Actuators, B* **1996**, *30*, 77−80. (d) McDonnell, J. M. *Curr. Opin. Chem. Biol.* **2001**, *5*, 572−577.

(17) Holland, W. R.; Hall, D. G. *Phys. Rev. B* **1983**, *27*, 7765−7768.

(18) Schultz, D. A. *Curr. Opin. Biotechnol.* **2003**, *14*, 13−22.

(19) (a) Lyon, L. A.; Musick, M. D.; Natan, M. J. *Anal. Chem.* **1998**, *70*, 5177−5183. (b) Englebienne, P.; Hoonacker, A. V.; Verhas, M. *Analyst* **2001**, *126*, 1645−1651.

(20) He, L.; Musick, M. D.; Nicewarner, S. R.; Salinas, F. G.; Benkovic, S. J.; Natan, M. J.; Keating, C. D. *J. Am. Chem. Soc.* **2000**, *122*, 9071−9077.

(21) Zayats, M.; Pogorelova, S. P.; Kharitonov, A. B.; Lioubashevski, O.; Katz, E.; Willner, I. *Chem. Eur. J.* **2003**, *9*, 6108−6114.

(22) (a) Henglein, A.; Lilie, J. *J. Am. Chem. Soc.* **1981**, *103*, 1059−1066. (b) Ung, T.; Giersig, M.; Dunstan, D.; Mulvaney, P. *Langmuir* **1997**, *13*, 1773−1782. (c) Templeton, A. C.; Pietron, J. J.; Murray, R. W.; Mulvaney, P. *J. Phys. Chem. B* **2000**, *104*, 564−570. (d) Mulvaney, P. *Langmuir* **1996**, *12*, 788−800.

(23) Zayats, M.; Kharitonov, A. B.; Pogorelova, S. P.; Lioubashevski, O.; Katz, E.; Willner, I. *J. Am. Chem. Soc.* **2003**, *125*, 16006−16014.

(24) Chidsey, C. E. D. *Science* **1991**, *251*, 919−922.

(25) Alvarez, M. M.; Khoury, J. T.; Schaaff, T. G.; Shafigullin, M. N.; Vezmar, I.; Whetten, R. L. *J. Phys. Chem. B* **1997**, *101*, 3706−3712.

On the other hand, the plasmon peak is unidentifiable for Au-NP of less than 2.0 nm effective diameter.[25] Therefore, changes in the electron density of these nanoparticles could not be traced by the shift in the peak position.

Here, we wish to report on the assembly of the biocatalyst glucose oxidase (GOx) on an array of Au-NPs, mean diameter 1.4 nm, coupled to a SPR-active Au-surface and the probing of the biocatalytic properties of the GOx/Au-NP hybrid by means of SPR spectroscopy. The observed shifts of the plasmon angle (angle of minimum reflectance) were interpreted as originating from the enzyme-induced charging of the Au-NP layer associated with the Au support. We demonstrate that the biocatalytic process in the presence of glucose charges the Au-NP, and that the charging process can be followed by SPR spectroscopy and by electrochemical means. To the best of our knowledge, this is the first example demonstrating the charging of metal nanoparticles with electrons by a biocatalytic process. Besides the fundamental interest of the system in the understanding of the "bio-pumping" of electrons into metallic NPs, the results have important practical implications in developing new biosensor configurations. The method allows us to trace the Au-NP charging event for such small Au-nanoparticles, that lack the characteristic absorbance peak.

Experimental Section

Materials. N^6-(2-Aminoethyl)-flavin adenine dinucleotide (amino-FAD, **1**) was synthesized and purified as described before.[26] Glucose oxidase (GOx, EC 1.1.3.4 from *Aspergillus niger*) was purchased from Sigma and used without further purification. Apo-glucose oxidase (apo-GOx) was prepared by a modification[10b] of the reported method.[27] Mono-sulfo-NHS-Nanogold (Au-nanoparticles functionalized with a single reactive group, a sulfo-*N*-hydroxysuccinimide ester that reacts with primary amines) was purchased from Nanoprobes, USA. Sulfo-*N*-hydroxy-succinimido-Au-nanoparticles, 6×10^{-5} M, were reacted with **1**, 6.8×10^{-4} M, in 0.03 M HEPES-buffer, pH 7.9, for 1 h at room temperature and then overnight at 4 °C. The **1**-functionalized Au-nanoparticle conjugate was purified from the excess of nonreacted **1** using a spin-column device (Spin Column-30, Sigma). The resulting conjugate was characterized by absorbance spectroscopy, and the ratio of **1** and the Au-nanoparticle in the **1**−Au-NP hybrid was found to be 1:1. The apo-GOx, 3 mg mL^{-1}, was reconstituted with the **1**-functionalized Au-nanoparticle conjugate, 4.8×10^{-6} M, in 0.1 M phosphate buffer, pH 7.0, that included 30% w/v glycerol, 0.1% w/v bovine serum albumin, 0.1% w/v sodium azide, for 4 h at room temperature and then overnight at 4 °C. The GOx reconstituted with the **1**-functionalized Au-nanoparticle was purified using a centrifugal filter (Centricon YM-100, Millipore). All other chemicals, including glucose, 1,2-benzene-dithiol (**2**), and 1,9-nonanedithiol (**3**), were purchased from Aldrich and used as supplied. Ultrapure water from Barnstead NANOpure Diamond source was used in all of the experiments.

The molecular dimensions of GOx were estimated using commercial software HyperChem (Release 2) for Windows. The protein structure was taken from the Protein Data Bank (Brookhaven National Laboratory).[28]

Modification of the Au-Electrode Surface. Glass supports (TF-1 glass, 20 × 20 mm) covered with a thin Cr sublayer (5 nm) and a polycrystalline Au layer (50 nm) supplied by Analytical-*μ*System were modified with Au-NPs functionalized with the reconstituted GOx. The

Au-coated plates were modified with the dithiols **2** or **3** by interacting the plates with ethanolic solutions of the respective dithiol, 10 mM, for 10 h, followed by rinsing of the electrodes with ethanol and water. The GOx−Au-NP hybrid consisting of GOx reconstituted on the **1**-functionalized Au-NPs, ca. 1×10^{-6} M, was adsorbed onto the dithiol-modified Au-electrode by interacting the modified electrode and GOx−Au-NPs in a phosphate buffer overnight at 4 °C.

In Situ Electrochemical-SPR Measurements. The surface plasmon resonance (SPR) Kretschmann type spectrometer Biosuplar-2 (Analytical-*μ*System, Germany, with a LED light source, $\lambda = 670$ nm, prism refraction index $n = 1.61$) was used in this work. The SPR data were processed using Biosuplar-2 software (version 2.2.30). The SPR sensograms (time-dependent changes of the reflectance minimum) represent real-time changes in the plasmon angle, and these were measured in situ using a home-built flow cell. Solutions of 0.1 M phosphate buffer, pH = 7.0, with various concentrations of glucose were degassed by flow of Ar and pumped through the cell (300 *μ*L) with a flow rate of 0.5 mL min^{-1}. The Au-covered glass plate was used as a working electrode (1.5-cm^2 area exposed to the solution) for the in situ electrochemical-SPR measurements. Auxiliary Pt and quasi-reference Ag electrodes made from wires of 0.5-mm diameter were parts of the cell. The Ag quasi-reference electrode was calibrated[29] according to the potential of dimethyl viologen (*N,N'*-dimethyl-4,4'-bipyridinium dichloride), $E° = -0.687$ V vs SCE, measured by cyclic voltammetry, and the potentials are reported vs SCE. Multipotential step experiments were performed using an electrochemical analyzer (EG&G, VersaStat) linked to a computer (EG&G Software #270/250). For the measurements of the generated voltages on the Au-electrode, a Keithley electrometer (model 617, input impedance greater than 40 TΩ) was used. Non-Faradaic impedance measurements were performed in the frequency range of 100 mHz to 10 kHz in 0.1 M phosphate buffer, pH = 7, under Ar using the electrochemical analyzer (model 6310, EG&G) connected to a personal computer (EG&G software 398). The experimental impedance spectra were fitted to the equivalent circuit consisting of the resistance and the constant phase element connected in series using a commercial software (Zview, version 2.1b, Scribner Associates Inc.). All of the measurements were carried out at ambient temperature (22 ± 2 °C).

Microgravimetric Measurements. A QCM analyzer (Fluke 164T multifunction counter, 1.3 GHz, TCXO) linked to a computer with the homemade software was used for microgravimetric measurements. Quartz crystals (AT-cut, ca. 9 MHz, EG&G) sandwiched between two Au-electrodes (geometrical area 0.2 cm^2, roughness factor ca. 3.5) were used. The Au-electrode surfaces were washed with ethanol and modified by the same way as described for Au-coated glass slides. Frequency changes of the quartz crystals were measured in air after each modification step. The QCM crystals were calibrated by electropolymerization of aniline in 0.1 M H_2SO_4 and 0.5 M Na_2SO_4 electrolyte solution, followed by coulometric assay of the resulting polyaniline film and relating the crystal frequency changes to the electrochemically derived polymer mass.

Results and Discussion

The reconstitution of apo-GOx on the flavin adenine dinucleotide (FAD)-functionalized Au-NP (1.4 nm) and the assembly of the GOx/Au-NP hybrid on a Au-electrode was reported to electrically contact the enzyme and the electrode support.[12] The reconstitution of the enzyme on the Au-NP aligns the FAD redox center with respect to the Au-NP relay unit in a configuration that allows electrical communication (vide infra). Scheme 1A outlines the method to prepare and assemble the GOx/Au-NP hybrid on the Au surface. The Au-NP (1.4 nm diameter)

(26) Bückmann, A. F.; Wray, V.; Stocker, A. In *Methods in Enzymology: Vitamins and Coenzymes*; McCormick, D. B., Ed.; Academic Press: Orlando, Fl, 1997; Vol. 280, Part 1, p 360.
(27) Morris, D. L.; Buckler, R. T. In *Methods in Enzymology*; Langone, J. J., Van Vunakis, H., Eds.; Academic Press: Orlando, FL, 1983; Vol. 92, Part E, pp 413−417.
(28) http://www.rcsb.org/pdb.

(29) Katz, E.; Schlereth, D. D.; Schmidt, H.-L. *J. Electroanal. Chem.* **1994**, *367*, 59−70.

Scheme 1. (A) Assembly of the Electrically Contacted Reconstituted GOx/Au-NP Systems on Au-Electrodes by Means of Dithiol Bridging Units; (B) Assembly of the Random Covalently Linked GOx/Au-NP System on the Au-Electrode
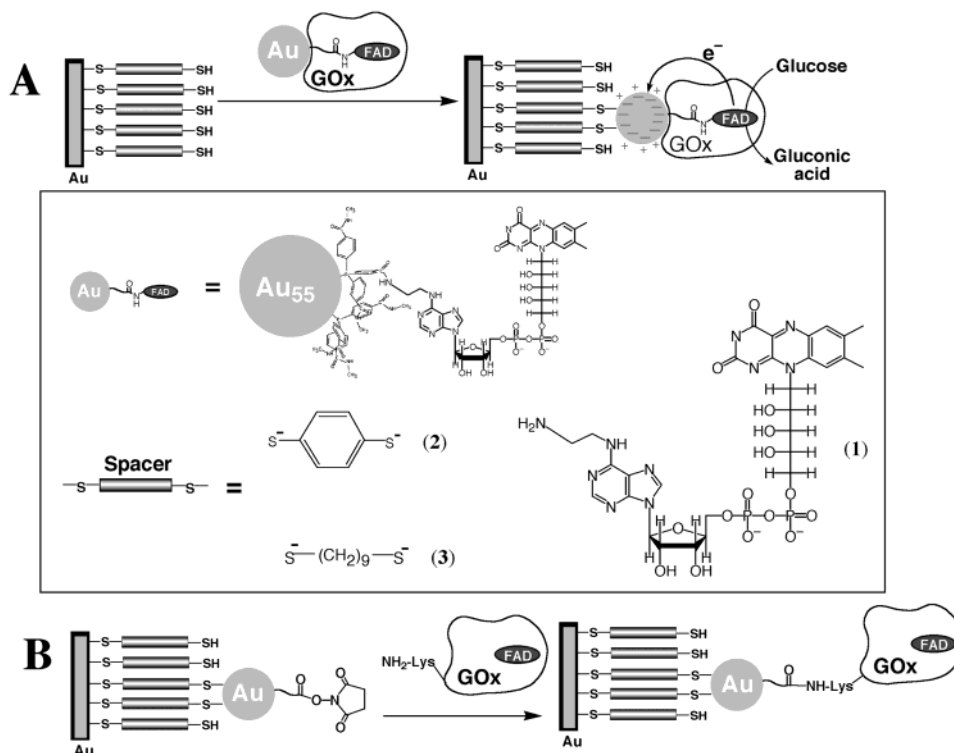
functionalized with a single *N*-hydroxysuccinimide ester group was reacted with the amino-FAD cofactor (**1**) to yield the FAD-functionalized Au-NP. The apo-GOx was reconstituted onto the modified Au-NP to yield the GOx/Au-NP hybrid. A monolayer of 1,4-benzenedithiol (**2**), a short dithiol, or of 1,9-nonanedithiol (**3**), a long dithiol, was assembled on the Au-surface, and this acted as a bridging film that binds the GOx/Au-NP system. Parallel microgravimetric quartz crystal microbalance (QCM) experiments indicate that the surface coverages of the short thiol (**2**) and of the long thiol (**3**) monolayer are ca. 1.1×10^{-10} and 2.5×10^{-10} mol cm^{-2}, respectively. The surface coverage of the GOx/Au-NP array in both systems was determined to be ca. 8.5×10^{-13} mol cm^{-2}, and this value translates to a surface coverage of 5.1×10^{11} hybrid species per cm^2. Taking into account the GOx average diameter of ca. 67 ± 5 Å, a densely packed monolayer of GOx exhibits a surface coverage of the enzyme corresponding to ca. 4.7×10^{-12} mol cm^{-2}. Thus, we conclude that the deposition of GOx/Au-NP yields ca. 30% of a 2D random densely packed GOx monolayer (ca. 60% of the ordered packing).[30]

The GOx/Au-NP hybrid system assembled on a Au-surface was characterized by in situ electrochemical-SPR spectroscopy. In the SPR experiments, the reflectivity, R, of the bulk gold layer is measured as a function of the incidence angle, θ, of the probe light ($R-\theta$ plot or SPR spectrum). The reflectivity varies as θ is changed, and it passes through a minimum value, R_{min}, at the plasmon angle, θ_P. The SPR spectrum can be characterized by three main values, θ_P, Γ_w, and R_{min}, where Γ_w is the width of SPR spectrum at a half of R well. Generally, changes in the SPR spectrum in response to the modification of the Au-

(30) (a) Finegold, L.; Donnell, J. T. *Nature* **1979**, *278*, 443−445. (b) Bourdillon, C.; Demaille, C.; Cueris, J.; Moiroux, J.; Savéant, J.-M. *J. Am. Chem. Soc.* **1993**, *115*, 12264−12269.

surface include a shift ($\Delta\theta_P$) of the θ_P value, as well as the changes of the reflectivity $\Delta R/R$ and the resonance curve width Γ_w. The changes occurring on the Au-support/solution interface can collectively or selectively alter the three SPR spectrum features ($\Delta\theta_P$, Γ_w, and $\Delta R/R$).

Figure 1A shows the SPR spectra of the GOx/Au-NP system bridged to the Au-support by the long dithiol (**3**) monolayer before the addition of glucose, curve a, and after the addition of different concentrations of glucose in the range of 3×10^{-4} to 1×10^{-2} M, curves b−f. Clearly, the plasmon angle θ_P shifts to higher values, and at a glucose concentration of 1×10^{-2} M the plasmon angle is shifted by $\Delta\theta_P = 39'$ (angle minutes), Figure 2A, curve a. Figure 1B shows the SPR spectra of the analogous system, that is bridged with the short dithiol (**2**) monolayer, before the addition of glucose, curve a, and after the addition of the same concentrations of glucose, curves b−e. As before, addition of glucose causes the shift of the plasmon angle θ_P to higher values, but the changes in the plasmon angles are smaller than those in the previous system ($\Delta\theta_P = 27'$ in the presence of 1×10^{-2} M glucose), Figure 2A, curve b. Figure 1C shows the SPR spectra corresponding to a control system, where GOx was covalently linked through lysine residues to the active ester-functionalized Au-NP, and the resulting GOx/Au-NP hybrid system was associated to the long dithiol (**3**) bridging monolayer, Scheme 1B. In this GOx/Au-NP system, the enzyme is immobilized in a nonaligned configuration, and previous studies have shown that the FAD center lacks electrical communication with the Au-NP in this randomly deposited enzyme.[12] From Figure 1C, one could conclude that the addition of glucose leads to a shift in the plasmon angle θ_P, but these shifts $\Delta\theta_P$ are substantially smaller than those observed for the structurally aligned GOx/Au-NP associated with the **3**-modified
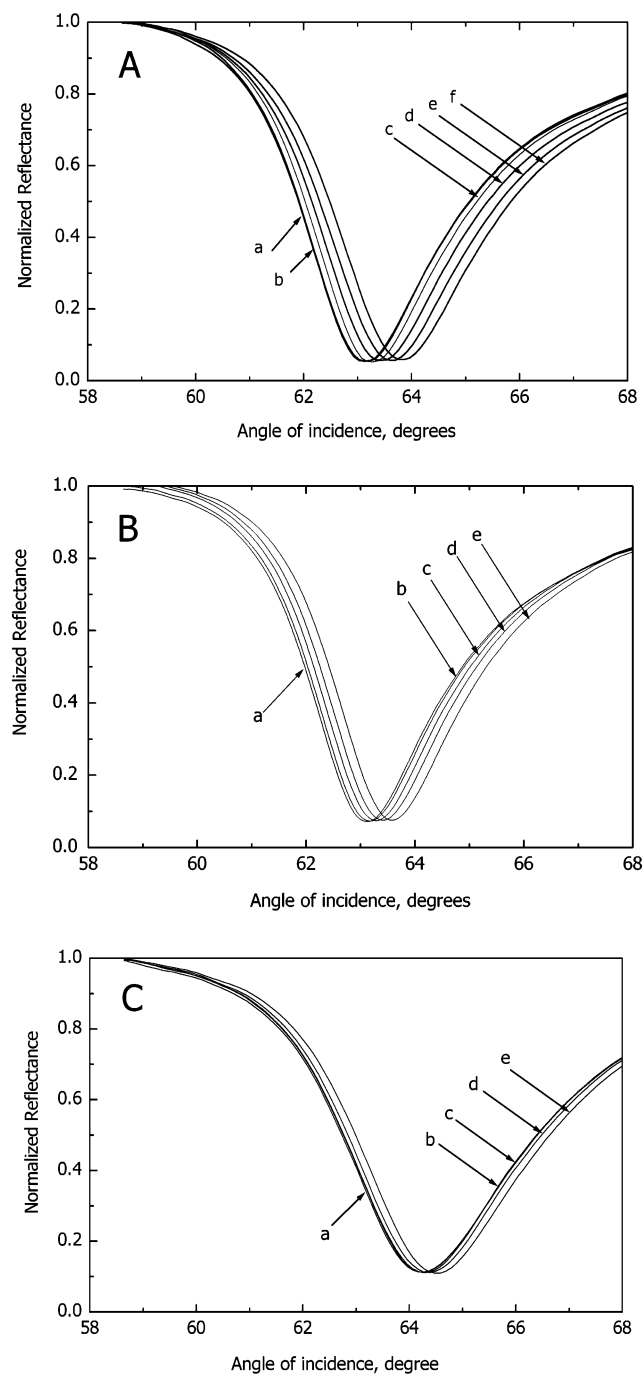
Figure 1. SPR spectra corresponding to the GOx-functionalized-Au-NP arrays bridged to the Au-electrodes with dithiol bridging units upon the addition of different concentrations of glucose: (a) 0 mM, (b) 0.3 mM, (c) 1.6 mM, (d) 8 mM, (e) 40 mM, (f) 100 mM. (A) Aligned GOx-reconstituted Au-NPs bridged to the Au-electrode with the long dithiol (**3**). (B) Aligned GOx-reconstituted Au-NPs bridged to the Au-electrode with the short dithiol (**2**). (C) Nonaligned GOx randomly covalently bound to the Au-NPs bridged to the Au-electrode with the long dithiol (**3**).

interface, Figure 2A, curve c. For example, at a glucose concentration of 1×10^{-2} M, the nonaligned system yields a change in the reflectivity angle of 14′ only, whereas the aligned GOx/Au-NP system associated with the **3**-monolayer leads to the change of $\Delta\theta_{P} = 39′$ under similar conditions.

To gain further understanding of the sources that lead to the shifts in the plasmon angles, we performed additional control experiments comparing the changes in the values of the plasmon angles upon treatment of the differently modified Au surfaces
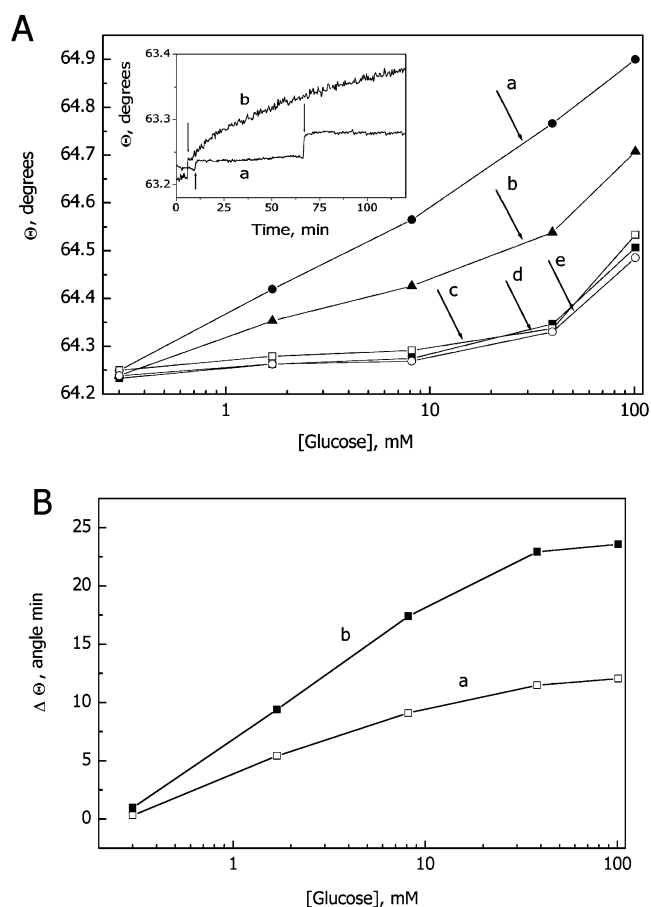

Figure 2. (A) Shifts of the plasmon angles induced upon addition of different concentrations of glucose to the following: (a) The aligned GOx-reconstituted Au-NPs bridged to the Au-electrode with the long dithiol (**3**). (b) The aligned GOx-reconstituted Au-NPs bridged to the Au-electrode with the short dithiol (**2**). (c) The nonaligned GOx randomly covalently bound to the Au-NPs bridged to the Au-electrode with the long dithiol (**3**). (d) The NP-array bridged to the Au-electrode with the long dithiol (**3**). (e) The Au-electrode surface modified with the long dithiol (**3**) monolayer. Inset: (a) Time-dependent changes of the plasmon angle of the nonaligned GOx/(**1**)-Au-NP system bridged with the long dithiol (**3**) monolayer upon the addition of 0.3 and 1.6 mM glucose (injection times are shown by the arrows). (b) Time-dependent changes of the plasmon angle of the aligned GOx/Au-NP system bridged with the long dithiol (**3**) monolayer upon the addition of 1.6 mM glucose (injection time is shown by the arrow). (B) The relative changes of the plasmon angle upon the addition of various glucose concentrations to the aligned GOx/Au-NP system bridged to the Au-electrode with: (a) the short dithiol linker (**2**), and (b) the long dithiol linker (**3**).

with various concentrations of glucose, Figure 2A. Curves e and d correspond to the changes in the plasmon angles of the Au-surface modified with the long dithiol (**3**) monolayer and to the **3**-modified surface functionalized with the **1**-derivatized Au-NPs upon the addition of different concentrations of glucose, respectively. Figure 2A, curve c, shows the changes in the values of the plasmon angles upon treatment of the **3**-modified Au surface functionalized with the nonaligned GOx/Au-NP system with different concentrations of glucose. Evidently, curve c overlaps with curves d and e, suggesting that the SPR spectrum changes in these systems originate only from the alteration of the refractive index of the solution containing different concentrations of glucose. On the other hand, the aligned GOx/Au-NP structures linked to the Au-surface through the short dithiol monolayer (**2**), curve b, or the long dithiol monolayer (**3**), curve a, reveal substantially higher changes in the values

of the plasmon angle shifts as compared to the changes originating from the alteration of the refractive index of the media upon addition of glucose. These enhanced changes in the plasmon angles are attributed to the charging of the particles by the biocatalytic process, Scheme 1A. The dithiol monolayer between the Au-NPs and the Au-surface introduces a barrier for transporting the electrons from the Au-NPs to the bulk Au-surface. Thus, because of a slow electron-transfer rate between the Au-NP and a Au-electrode, electrons are effectively stored on the Au-NP, leading to their steady-state charging. This changes the dielectric constant of the interface, leading to the plasmon angle shifts (vide infra). Figure 2A, inset, shows the different types of the time-dependence profiles of the plasmon angle changes upon addition of glucose to the systems consisting of the aligned and nonaligned GOx/Au-NP arrays bridged to the Au-surface by the long dithiol (**3**). Curve a corresponds to the nonaligned GOx/Au-NP system and shows the θ_P shift upon stepwise addition of glucose with concentrations of 3×10^{-4} and 1.6×10^{-3} M (the time at which glucose is injected is marked with arrows). The observed fast changes of the θ_P result from the immediate alteration of the refractive index of the bulk solution upon glucose addition. Curve b corresponds to the time-dependent changes of θ_P in the aligned GOx/Au-NP system upon the addition of glucose. It shows the same fast change of the θ_P after glucose addition, 1.6×10^{-3} M (shown by the arrow), followed by a large gradual shift of θ_P that tends to level-off to a steady-state value. The observed gradual rise of θ_P, curve b, reflects a different mechanism that affects the changes in θ_P, that occurs only in the aligned GOx/Au-NP system upon addition of glucose. While the instantaneous increase in the θ_P value is attributed to the change in the refractive index of the medium upon the addition of glucose, the subsequent slow changes in the θ_P values are attributed to the charging of the Au-NPs by the biocatalytic process. This charging process is slow because it involves the charging of the particles by the biocatalytic process and the discharging of the Au-NPs by tunneling the electrons to the bulk Au-support, the process that leads to a steady-state equilibrium charging of the Au-NPs.

Figure 2B shows the net relative changes $\Delta\theta_P$ of the plasmon angles originating from the charging of the Au-NPs in the systems consisting of the aligned GOx/Au-NP system associated with the short dithiol (**2**) on the Au-surface, curve a, and with the long dithiol (**3**) on the Au-surface, curve b, at different concentrations of glucose. These curves were obtained by the subtraction of the changes in the plasmon angles originating from the alteration of the refractive index of the bulk solution at variable glucose concentration, Figure 2A, curve c, from the total plasmon shifts observed in the systems consisting of the aligned GOx/Au-NPs linked to the Au-surface by the spacers **2** or **3**, Figure 2A, curves b and a, respectively. It is clear that the changes of the plasmon angles increase upon elevating the glucose concentrations, and that the changes tend to level-off at a glucose concentration of ca. 1×10^{-2} M. Also, the changes in the plasmon angles are more pronounced in the long dithiol system, as compared to the short dithiol system. For example, at a glucose concentration that corresponds to 1×10^{-2} M, the GOx/Au-NP bridged to the **2**-functionalized Au surface reveals a value of $\Delta\theta_P = 12'$, whereas the GOx/Au-NP system linked

to the **3**-modified Au-surface reveals a plasmon angle shift of value $\Delta\theta_P = 23.6'$.

These extra changes in the plasmon angles upon addition of glucose in solution, beyond the changes induced by the bulk solution refractive index, are attributed to the biocatalytic charging of the Au-NP, Scheme 1A. The aligned GOx/Au-NP exhibits electrical communication between the enzyme and the Au-NP. This enables the catalyzed oxidation of glucose that results in the transfer of electrons to the Au-NP. Recently, current−voltage measurements of charge transport through molecules self-assembled onto gold electrodes revealed resistance values of the interfaces that corresponded to ca. 2.2×10^7 and to ca. 5×10^8 Ω, for 1,4-benzenedithiol (**2**)[31] and for 1,9-nonanedithiol (**3**)[32] monolayers, respectively. Also, previous electrochemical studies have indicated that 1,4-benzenedithiol exhibits a relatively low tunneling barrier, whereas 1,9-nonanedithiol reveals a high tunneling barrier for the electron transfer from the Au-NP to the Au-electrode.[12] As a result, the steady-state charging degree of the Au-NP is expected to be higher in the presence of the long dithiol (**3**) monolayer. This is reflected by the enhanced shifts in the SPR spectra of the aligned GOx/Au-NP system linked to the electrode by the **3**-monolayer.

From Figures 1 and 2, one can realize that the relative changes in $\Delta R/R$ and Γ_w are much smaller than the changes in the plasmon angle, θ_P. Thus, by analyzing the SPR spectra, we conclude that the plasmon angle, θ_P, could be selected as the parameter describing the main changes in the studied systems. Usually, the shift in the plasmon angle, which is not accompanied by changes in reflectivity, is related to an increase in the real part of the corresponding dielectric constant, ϵ_1. In the case of many metals, their dielectric properties are well described by the simple free electron Drude model.[33] According to this model, the response of a metal to an electromagnetic field of angular frequency ω is described by the dielectric constant $\epsilon(\omega) = \epsilon'(\omega) + i\epsilon''(\omega)$ that includes the real and imaginary parts, respectively, and it may be written as eq 1:

$$\epsilon(\omega) = 1 - \frac{\omega_p^2}{\omega_d^2 + \omega^2} + i \frac{\omega_p^2 \omega_d}{\omega(\omega_d^2 + \omega^2)} \tag{1}$$

where ω_p is the bulk plasma frequency and ω_d is the damping frequency, related to the mean free path of the conduction electrons in the bulk. Gold can be considered as a free electron like metal for light wavelength above 600 nm, and thus a simplified expression for the real part of $\epsilon(\omega)$ can be formulated in the form of eq 2:

$$\epsilon'(\omega) = \frac{\omega_p^2}{\omega_d^2 + \omega^2} \tag{2}$$

where the plasma frequency ω_p is proportional to the density of electrons, N, eq 3:

$$\omega_p^2 = Ne^2/m\epsilon_0 \tag{3}$$

(31) Reed, M. A.; Zhou, C.; Muller, C. J.; Burgin, T. P.; Tour, J. M. *Science* **1997**, *278*, 252−253.
(32) Beebe, J. M.; Engelkes, V. B.; Miller, L. L.; Frisbie, C. D. *J. Am. Chem. Soc.* **2002**, *124*, 11268−11269.
(33) Ashcroft, N. W.; Mermin, N. D. *Solid State Physics*; Holt, Rinehart and Wiston: New York, 1976.

where e is the electron charge, m is the effective mass of the electron, and ϵ_0 is the permittivity of free space.

Importantly, the dielectric constant of metals depends on the plasma frequency ω_p, eq 1, and, therefore, on the density of the conduction electrons, N. Therefore, when the biocatalyzed transfer of electrons into the particle occurs, the density of the free electrons, N, is increased, probably near the particle surface (Thomson−Fermi layer), and consequently the dielectric constant, $\epsilon'(\omega)$, is altered according to eq 4:

$$\Delta\epsilon'(\omega)/\epsilon'(\omega) \approx \Delta N/N \qquad (4)$$

where ΔN is the change in the density of electrons in the Au-NP.

It is known that the SPR angular shift $\Delta\Theta_p$ is a function of the immobilized layer thickness and of the optical (dielectrical) difference of the layer as compared to the surrounding medium, $\epsilon_{layer} - \epsilon_{solution}$.[14a] The changes in the dielectric constant of the Au-NP layer will result in the changes in the dielectric constant of the interface and will lead to the shifts in the plasmon angle position. Thus, the steady-state charging of the Au-nanoparticles with the GOx-generated electrons, and the change of the dielectric constant of the Au-NP layer, could lead to the enhanced plasmon angle shifts observed in the pesent study. Hence, changes in the electron density of Au-NPs with an effective diameter that is less than 2.0 nm, which do not exhibit a plasmon peak in the optical spectrum,[25] could be traced by the shift in the SPR plasmon angle position.

Previous studies monitored changes in the plasmon band position of Au-NPs as a result of electrochemical charging.[22] In the present study, we follow, however, the charging effects on the coupling between the LP of the Au-NP and the SP wave of the gold interface. Furthermore, our study reveals the unique charging of the Au-NPs by a biocatalytic process.

For further understanding of the Au-NP charging mechanism, double-layer differential capacitances, C_{dl}, of the interfaces composed of the aligned GOx/Au-NP systems on the dithiol-functionalized Au-surfaces were derived from non-Faradaic impedance spectra measurements.[34] The impedance spectra were fitted to the equivalent circuit composed of a constant phase element (CPE), eq 5:

$$CPE = A^{-1}(j\omega)^{-n} \qquad (5)$$

where the physical meaning of A depends on the value of the parameter n, and ω is the frequency of the alternative voltage. The constant phase element reflects nonhomogeneity of the layer, and the extent of its deviation from the capacitance is controlled by the parameter n in eq 5. The CPE has the meaning of capacitance, and the coefficient A becomes equal to the C_{dl} when $n = 1$.[34] For the GOx/Au-NP system on the dithiol-functionalized Au-surfaces, the value for n was found to be ca. 0.93, and thus the CPE was considered as mainly capacitance. The value of the interfacial differential capacitance, C_{dl}, in the absence of glucose was found to be ca. 2.1 and 19.1 μF cm^{-2} for the long dithiol (**3**) and the short dithiol (**2**), respectively. This is consistent with the fact that the long dithiol forms a

dense hydrophobic monolayer, whereas the short dithiol monolayer includes pinholes that allow the permeation of water molecules into the monolayer structure.

Charging of the Au-NPs associated with the interface should result in changes of the double-layer capacitance. For example, in the recent electrochemical studies on self-assembled monolayers functionalized with ionizable headgroups, the influence of the degree of ionization of the terminal headgroups on the interfacial capacitance was demonstrated.[35] The charge accumulation in the double-layer upon ionization of acidic or basic groups associated with the monolayer resulted in the increase of the total interfacial capacitance, and this was confirmed by impedance spectra measurements.[36] The potentials of the GOx/Au-NP-modified electrodes, prior to the addition of glucose, are close to the zero-charge potential (E_{zcp}) values and thus provide the minimum values of C_{dl}. Upon the addition of glucose, the biocatalyzed charging of the Au-NPs results in a negative potential shift versus the initial E_{zcp}, and this is anticipated to yield an increase in C_{dl}. Indeed, the expected increase of the C_{dl} upon the biocatalyzed glucose oxidation was experimentally observed in the presence of the aligned GOx/Au-NP system. The time-dependent changes of the C_{dl} upon addition of glucose to the system were followed by the impedance measurements at a fixed frequency $f = 1$ kHz ($\omega = 2\pi f$). Figure 3A, curve a, shows the time-dependent differential capacitance changes of the aligned GOx/Au-NP system bridged to the Au-electrode by the long dithiol (**3**) upon the addition of 100 mM of glucose. The capacitance increases from ca. 2.1 to 3.6 μF cm^{-2}. The time-profile of the differential capacitance changes is very similar to the time-dependence of the plasmon angle shifts upon addition of glucose, Figure 2A, inset, curve b, suggesting that the parameters originate from the same phenomenon in the system (the biocatalyzed charging of the Au-NPs). The extent of the capacitance increase is dependent on the glucose concentration. Figure 3A, inset, shows the capacitance increase, ΔC_{dl}, as a function of the concentration of added glucose to the system consisting of the aligned GOx/Au-NPs bridged to the Au-electrode by the long dithiol linker (**3**). For comparison, Figure 3A, curve b, shows the capacitance of the nonaligned GOx/Au-NP system linked by **3** to the Au-surface. Clearly, no capacitance changes occur on the interface of the nonaligned GOx/Au-NP system, indicating that no biocatalyzed charging of the Au-NP takes place. These results are consistent with the SPR experiments. Figure 3B shows the results of the same experiment upon following the capacitance changes of the aligned GOx/Au-NP system linked to the Au surface by the short dithiol (**2**) monolayer in the presence of added glucose, 100 mM, curve a. The capacitance increases from ca. 19 to 24.7 μF cm^{-2}. Similarly, the nonaligned GOx/Au-NP does not reveal any significant changes in the capacitance of the system upon the addition of glucose, Figure 3B, curve b. The results observed with the nonaligned GOx/Au-NP systems imply that the added glucose has no effect on the capacitance of the system. Also, we see that the initial capacitance of the **3**-bridged system, 2.1 μF cm^{-2}, prior to the addition of glucose, is substantially lower than the capacitance of the **2**-bridged GOx/Au-NP system, ca. 19 μF cm^{-2}. It is interesting to note that

(34) (a) Bard, A. J.; Faulkner, L. R. *Electrochemical Methods: Fundamentals and Applications*; Wiley: New York, 1980. (b) Stoynov, Z. B.; Grafov, B. M.; Savova-Stoynova, B. S.; Elkin, V. V. *Electrochemical Impedance*; Nauka: Moscow, 1991. (c) Katz, E.; Willner, I. *Electroanalysis* **2003**, *15*, 913−947.

(35) (a) Smith, C. P.; White, H. S. *Langmuir* **1993**, *9*, 1−3. (b) Andreu, R.; Fawcett, W. R. *J. Phys. Chem.* **1994**, *98*, 12753−12758.
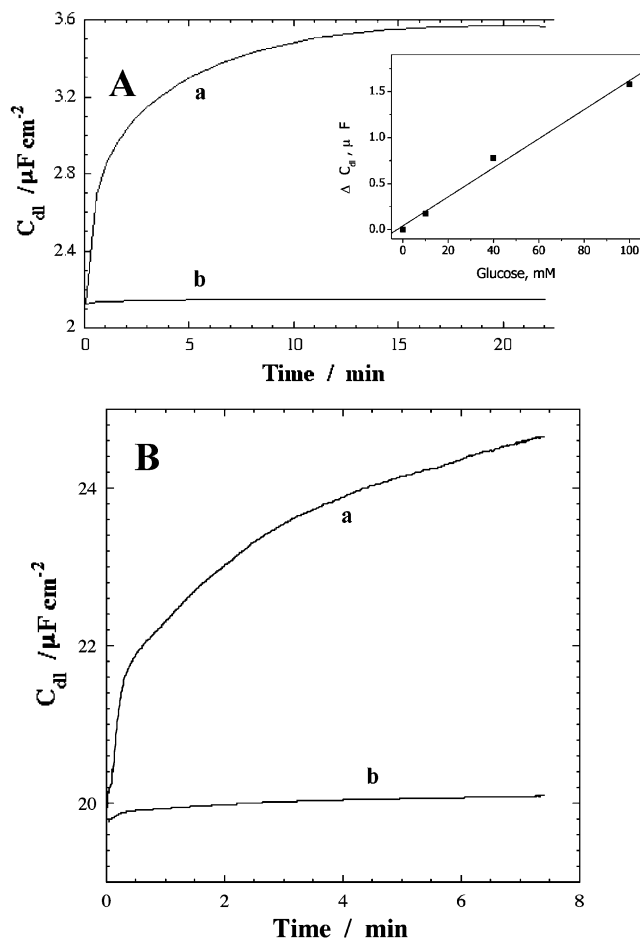(36) Schweiss, R.; Werner, C.; Knoll, W. *J. Electroanal. Chem.* **2003**, *540*, 145−151.

Figure 3. (A) Time-dependent capacitance changes of the GOx/Au-NP system bridged by the long dithiol (**3**) upon the addition of 100 mM glucose: (a) The aligned GOx/Au-NP system. (b) The nonaligned GOx/Au-NP system. Inset: Effect of various concentrations of glucose on the capacitance values of the aligned GOx/Au-NP system bridged to the electrode with the long dithiol (**3**). (B) Time-dependent capacitance changes of the GOx/Au-NP system bridged to the electrode by the dithiol, (**2**), upon the addition of 100 mM glucose: (a) The aligned GOx/Au-NP system. (b) The nonaligned GOx/Au-NP system. The concentration of glucose was equal to 100 mM.

upon addition of glucose, 100 mM, to the **3**-bridged aligned GOx/Au-NP system, the capacitance increases by ca. 80% to ca. 3.6 μF cm^{-2}, whereas in the **2**-bridged aligned GOx/Au-NP system the capacitance increases only by ca. 22% to the value of 24.7 μF cm^{-2}. These results are consistent with the larger shift of θ_P observed in the SPR measurements in the presence of the long dithiol linker (**3**) as compared to the changes observed with linker **2**. That is, the long dithiol linker (**3**) yields a densely packed monolayer that provides an effective tunneling barrier for the transport of electrons from the Au-NPs to the bulk Au-electrode. This results in the effective charging of the Au-NPs that is reflected by the significant changes of the interfacial capacitance. In contrast, the short dithiol linker (**2**) allows the leakage of electrons from the Au-NPs to the bulk Au-electrode, resulting in the diminished charging of the Au-NPs. Accordingly, only moderate changes in the capacitance values of the interface are observed.

We have further employed potentiometric measurements to explore the nature of the charging processes of the Au-NPs. In these experiments, the potentials, E_G, generated on the bulk Au-electrode functionalized with the aligned GOx/Au-NPs and
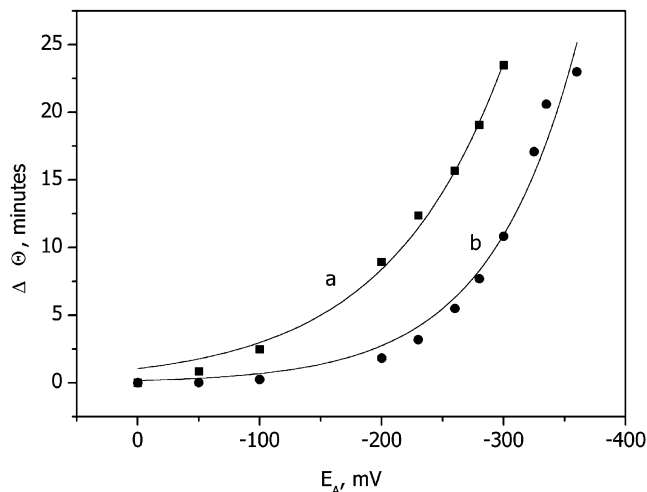

Figure 4. Changes in the plasmon angle upon the application of variable potentials on the Au-electrode modified with the GOx/Au-NP array in the absence of glucose in solution: (a) The system bridged by the short dithiol (**2**) monolayer. (b) The system bridged by the long dithiol (**3**) monolayer.

linked to the Au-electrode by spacer **2** or **3** were measured in the presence of different concentrations of glucose. For example, upon addition of glucose, 8 and 100 mM, to the long dithiol-bridged aligned GOx/Au-NP system, the measured electrode potentials, E_G, corresponded to -15 and -33 mV (vs SCE), respectively.

Provided that the biocatalytic charging of the Au-NP core leads to the observed shifts in the plasmon angles, that are accompanied by the changes in C_{dl} and E_G, one may perform the reverse experiments where a negative potential is applied on the same electrode that contains the GOx/Au-NP array organized on either the **2** or the **3** spacer to charge the Au-NP electrochemically. The charging of the Au-NPs by the external potential is then monitored by the changes in the plasmon shifts in the SPR spectra. The potential of the modified Au-electrode, E_A, was controlled by a potentiostat with the use of a counter electrode and a SCE reference electrode, and the SPR measurements were performed for each potential applied on the modified Au-electrode. Figure 4 shows the changes in the plasmon angles, θ_P, of the GOx/Au-NP systems linked to the surface by linker **2** or **3** at different applied potentials. For example, the plasmon angle shifts, $\Delta\theta_P$, similar to those observed in the presence of 100 mM of glucose, were generated upon the application of the potentials E_A of -230 and -360 mV (vs SCE) on the **2** and **3** dithiol-bridged GOx/Au-NP systems, respectively. It should be noted that application of the potential of -360 mV (vs SCE) on the Au-electrode coated with the **3**-monolayer which lacks the Au-NPs yields only a minute shift of θ_P, ca. 2.6′. Thus, we believe that the observed changes in the plasmon angle of the samples containing the Au-NP array originate from the charging of the Au-NPs as a result of the application of the negative potential to the electrode. Under the externally applied potential on the bulk electrode, electron tunneling to the Au-NP layer will occur, and the charging of the Au-NPs will proceed until the potential equilibrium between the Au-electrode and the Au-NP-layer will be established. Charging of the Au-NPs alters their plasmon frequency, and therefore the dielectric constant of the particles and the whole interface, and this leads to the changes in the plasmon angle. While upon addition of 100 mM of glucose to the solution the aligned GOx/Au-NP array

bridged via the long dithiol (**3**) layer, the potential, E_G, generated on the bulk electrode is -33 mV, a potential of -360 mV has to be applied on the bulk electrode to gain a similar change in the plasmon angle of the system in the absence of glucose. Thus, one may conclude that a potential drop, ΔV, across the dithiol layer between the bulk Au-electrode and the Au-NPs results in this potential difference.

Thus, the biocatalytic process and the external applied potential can charge independently the GOx/Au-NP interface. The extent of charging is imaged by the changes in the plasmon angle shifts. The charging process is, however, observed because of the existence of the molecular barrier between the GOx/Au-NPs and the electrode that leads to the potential drop accross the interface. The results indicate that the potential drop across the long dithiol (**3**) monolayer is higher than that across the short dithiol (**2**) monolayer.

When the electrode is charged and electrostatic equilibrium is attained, the charge on the electrode is balanced by the opposite charge in the solution. The charge separation and the total interfacial capacitance, K_{total}, can be described by three capacitors in series: the integral capacity of the thiol layer, K_{th}, the integral capacity of the Stern layer, K_{St}, and the integral capacity of the diffuse layer, K_d, extending into the bulk of the electrolyte, eq 6:[37]

$$\frac{1}{K_{total}} = \frac{1}{K_{th}} + \frac{1}{K_{St}} + \frac{1}{K_D} \quad (6)$$

The integral capacitance of the Stern layer, K_{St}, is provided by the electrolyte ions in the close vicinity to the external interface of the dithiol monolayer and includes the double charged layer around the Au-NPs.

Assuming that there is no charge in the film except that associated with the Au-NP, the potential decays linearly from the metal, E_M, to the Au-NP layer, E_{NP}, or vice versa, depending on the potential source. The potential drop, ΔV, across the dithiol layer is proportional to the ratio of the charge density on the surface of the electrode, σ_M, and the integral capacitance of the layer, K_{th}, eq 7:[37]

$$\Delta V = E_A - E_{NP} = \sigma_M K_{th}^{-1} \quad (7)$$

where E_A is a potential of the bulk Au-electrode applied by the potentiostat, E_{NP} is the potential of the Au-NP array, $K_{th} = \epsilon_0\epsilon_1/d_1$, and d_1 is the dithiol monolayer thickness. The potential applied on the Au-electrode using a potentiostat results in the respective alteration of the charge density, σ_M, in the metal. Because the potential drop across the dithiol monolayer, ΔV, is proportional to the excess charge density on the surface of the Au-electrode, this will result in the corresponding change of the Au-NP layer potential. The potential applied on the bulk Au-electrode, E_A, is always higher than the potential E_{NP} produced on the Au-NP array (the difference is ΔV). The same potential difference, ΔV, is formed between the Au-NP array and the Au-electrode upon the biocatalytic charging of the Au-NPs, yet in this case the potential on the Au-NPs, E_{NP}, is larger than the potential generated on the Au-electrode, E_G, eq 8:

$$\Delta V = E_{NP} - E_G \quad (8)$$

Assuming the equal potential drop ΔV for any studied source of the potential (generated biocatalytically on the Au-NPs or
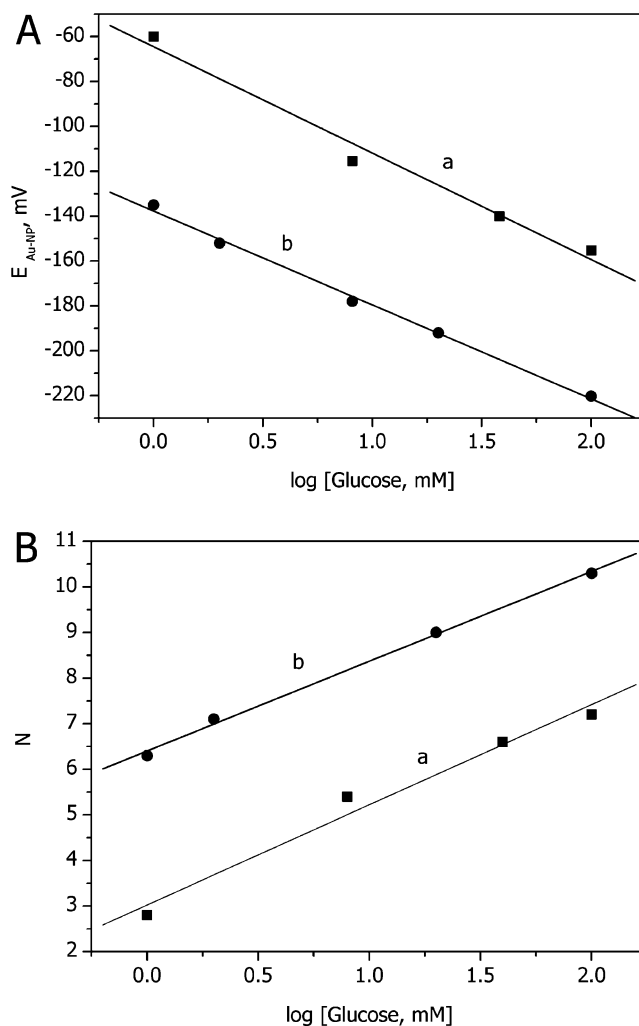
Figure 5. (A) Calculated enzyme-generated potentials on the Au-NP as a function of the logarithm of the glucose concentration for the short (a) and the long (b) dithiol bridging monolayers, respectively. (B) Dependence of the number of stored electrons per Au-NP as a function of the logarithm of the glucose concentration for the short (a) and the long (b) dithiol bridging monolayers.

applied electrochemically on the Au-electrode), we can calculate the potential on the Au-NP, E_{NP}, generated either by the enzyme-induced process or by the applied potential in the absence of glucose, that yields the same plasmon angle shifts. Combining eqs 7 and 8, one could derive the expression of ΔV via the two experimentally measured potentials E_G and E_A, eq 9:

$$\Delta V = (E_A - E_G)/2 \quad (9)$$

This allows calculation of the potential formed on the Au-NPs, eq 10:

$$E_{NP} = E_G + (E_A - E_G)/2 \quad (10)$$

Figure 5A shows the calculated values of E_{NP} (using eq 10) formed on the Au-NP bridged to the Au-electrode with the short dithiol (**2**), curve a, or with the long dithiol (**3**), curve b, upon the biocatalyzed oxidation of glucose by the aligned GOx/Au-NP assembly in the presence of different concentrations of

(37) Delahay, P. *Double Layer and Electrode Kinetics*; Wiley-Interscience: New York, 1965; Chapter 3 and references therein.

glucose. The two systems reveal linear dependencies with the similar slopes: $\delta E_{NP}/\delta(\log[\text{glucose}]) = 44 \pm 3$ mV per decade. This indicates that a similar charging mechanism occurs in the two systems. On the other hand, the calculated potential values biocatalytically generated on the Au-NPs bridged to the Au-electrode with the long dithiol (**3**) are higher by ca. 70 mV in comparison to the system based on the short dithiol (**2**) for each glucose concentration. This is consistent with the fact that the longer spacer provides a higher barrier for the electron leakage from the Au-NPs, thus preserving a higher charge density on the particles and resulting in a higher potential on the Au-NPs. Because the Au-NPs behave as molecules with multi-redox centers,[38] the charge accumulated on the Au-NP array, σ_p, should be proportional to the number of electrons in a single particle, N, accumulated under steady-state conditions, and the surface charge density of the layer could be expressed by eq 11:

$$\sigma_p = F\Gamma_{NP}N \quad (11)$$

where F is Faraday's number, and Γ_{NP} is the surface coverage of the Au-NP.

As a next step, we made an effort to quantitatively estimate the degree of charging of the Au-NPs by the biocatalytic process. An ionic charge layer is formed around the Au-NP core, and it is separated from the core by the capping organic monolayer that serves as a dielectric medium of the double-layer capacitor. In the studies of Murray and co-workers,[13] it was reported that the double-layer capacitance of a monolayer-capped Au-NP in an electrolyte solution is well described by the simple concentric sphere model of a capacitor, eq 12:

$$C_{AuNP} = 4\pi\epsilon\epsilon_0 r(r+d)/d \quad (12)$$

where C_{AuNP} is the capacitance of an individual Au-NP, r is the metal core radius, and ϵ and d are the static dielectric constant and the thickness of the capping monolayer, respectively. We apply this model to the Au-NPs studied in the present work that exhibit a core diameter of 1.4 nm and a phosphine monolayer capping of a thickness that corresponds to ca. 0.5 nm. Using a value for the dielectric constant of the phosphine layer of ca. 40,[39] we obtained an integrated capacitance that corresponded to ca. $K_{AuNP} = 7.5$ aF for a single Au-NP. Thus, a storage of a single electron on the Au-NP of that capacitance will change its potential by a step corresponding to $\Delta V = e/K_{AuNP} = 21$ mV, where e is the charge of the electron (1.602×10^{-19} C).

To extract the average number of electrons that are accumulated on an individual nanoparticle, one has to calculate the potential generated on a single nanoparticle and translate it to the number of electrons per particle using the calculated integral capacitance, K_{AuNP} (assuming that this capacitance is independent of the charging degree of the Au-NP). The potential E_{NP} is generated by the charge Q ($K_{AuNP} = Q/E_{NP}$), accumulated on the Au-NP, that is proportional to the number of electrons

in the particle, N, stored under steady-state conditions, where $Q = Ne$. Figure 5B shows the dependence of the number of stored electrons per Au-NP as a function of the logarithm of glucose concentration in solution for the short and for the long dithiol monolayers, curves a and b, respectively. Evidently, at a glucose concentration of 1×10^{-2} M, we estimate that ca. 10 electrons could be stored per Au-NP in the presence of the aligned GOx/Au-NP system which is bridged to the bulk Au-electrode by the long dithiol (**3**). Also, we find that the number of electrons charging the Au-NPs is strongly influenced by the molecular bridge that links the GOx/Au-NP hybrid to the bulk Au-electrode. For example, for a glucose concentration of ca. 1×10^{-2} M, the Au-NPs are charged with 6 and 10 electrons in the presence of linker **2** or **3**, respectively. That is, the nature of the molecular bridge that links the GOX/Au-NPs to the electrode and the extent of electron leakage through this tunneling barrier control the extent of charging of the Au-NPs.

Conclusions

The present study has demonstrated a new phenomenon in bioelectronics that involves the biocatalytic charging of Au-NPs associated with self-assembled monolayers on surfaces and the read-out of the charging process by means of surface plasmon resonance spectroscopy and electrochemical means (potentiometric and capacitance measurements). Besides the basic understanding of the biocatalytic pumping of electrons into Au-NPs, the phenomenon has important practical implications as it reveals new transduction methods.

Until now, redox enzymes were mainly applied for the developing of amperometric biosensors. A few potentiometric biosensors that use redox enzymes are available, yet these biosensors analyze indirectly the reaction substrate or the product (e.g., depletion of O_2 or changes in pH). The uniqueness of the present study is the introduction of a new biosensing principle that combines electrochemical processes and changes in the optical properties of the sensing interface occurring as a result of the bioelectrocatalytic transformation. These changes could be monitored only by application of tailored metal nanoparticles/reconstituted enzyme hybride systems.

To accomplish the biocatalytic charging of the nanoparticles, two prerequisites must be met: (i) The redox enzyme (in the present study GOx) should be electrically contacted with the Au-NPs. This is accomplished by the reconstitution of apo-GOx on the FAD-functionalized Au-NP, a process that orients and aligns the redox center of the enzyme with respect to the Au-NP. (ii) The enzyme/Au-NP hybrid system must be linked to a bulk Au-surface by dielectric long-chain molecular bridging units. This molecular bridging element provides a tunneling barrier for the transport of electrons from the Au-NPs to the bulk Au-electrode. This tunneling barrier results in the steady-state equilibrium accumulation of electrons in the Au-NPs.

The biocatalytic oxidation of glucose results in the transfer of electrons from the enzyme FAD-center to the Au-NPs, and the steady-state charging of the Au-NPs is controlled by two parameters: (i) the concentration of glucose, and (ii) the length of the molecular bridging unit acting as a tunneling barrier in the systems. While the short-chain bridging unit, 1,4-benzene-dithiol (**2**), exhibits a low tunneling barrier and thus leads to the inefficient charging of the Au-NPs, the long-chain bridging unit, 1,9-nonanedithiol (**3**), yields a high tunneling barrier and an effective charging of the Au-NPs.

(38) Wuelfing, W. P.; Green, S. J.; Pietron, J. J.; Cliffel, D. E.; Murray, R. W. *J. Am. Chem. Soc.* **2000**, *122*, 11465−11472.
(39) The capping monolayer consists of triphenylphosphine moieties, and each phenyl group holds a methylamide function. The dielectric constant of the triphenylphosphine moieties could be estimated as ca. 20, whereas the polar methylamide function has a very high dielectric constant that corresponds to ca. 180. The nondensely packed capping monolayer should also include some amount of water molecules. Also, the exact calculation of the effective value of the dielectric constant is impossible; we used the value of 40 as a rough approximation of the dielectric constant for the capping monolayer.

The biocatalytic charging of the Au-NPs alters the plasma frequency, and as a result changes the dielectric constant of the Au-NPs. The changes in the dielectric constant of the Au-NPs alter the dielectric properties of the whole interface, resulting in the pronounced shifts in the surface plasmon resonance (SPR) minimum reflectivity. The biocatalytic pumping of electrons into the Au-NPs was also characterized by electrochemical means. We find that the capacitance of the electrode increases upon the biocatalytic charging of the electrode interface, and the charging process could be also detected potentiometrically by monitoring the electrode potential.

The charging of the Au-NPs was also accomplished by the application of an external potential on the bulk electrode and by monitoring of the charging process by following the changes in the dielectric properties of the interface by means of SPR. Thus, surface plasmon resonance spectroscopy provides a new optical means to observe both biocatalytic and electrochemical charging of Au-NPs, even for the Au-NPs, which do not exhibit the plasmon peak in the optical spectrum. By the analysis of the experimental data, we were able to estimate the average number of electrons charging the Au-NPs at different glucose concentrations for the two different dithiol linkers.

JA049275V